Atmos. Chem. Phys. Discuss., 15, 34407–34437, 2015
www.atmos-chem-phys-discuss.net/15/34407/2015/
doi:10.5194/acpd-15-34407-2015

Atmospheric Chemistry and Physics Discussions

Impact of major volcanic eruptions on stratospheric water vapour

M. Löffler, S. Brinkop, and P. Jöckel

Deutsches Zentrum für Luft- und Raumfahrt (DLR), Institut für Physik der Atmosphäre, Oberpfaffenhofen, Germany

Received: 26 November 2015 – Accepted: 29 November 2015 – Published: 8 December 2015

Correspondence to: P. Jöckel (patrick.joeckel@dlr.de)

Published by Copernicus Publications on behalf of the European Geosciences Union.

Abstract

Volcanic eruptions can have significant impact on the earth's weather and climate system. Besides the subsequent tropospheric changes also the stratosphere is influenced by large eruptions. Here changes in stratospheric water vapour after the two major volcanic eruptions of El Chichón in Mexico in 1982 and Mount Pinatubo on the Philippines in 1991 are investigated with chemistry-climate model simulations. This study is based on two simulations with specified dynamics of the EMAC model, performed within the Earth System Chemistry integrated Modelling (ESCiMo) project, of which only one includes the volcanic forcing through prescribed aerosol optical properties. The results show a significant increase in stratospheric water vapour after the eruptions, resulting from increased heating rates and the subsequent changes in stratospheric and tropopause temperatures in the tropics. The tropical vertical advection and the South Asian summer monsoon are identified as important sources for the additional water vapour in the stratosphere. Additionally, volcanic influences on the tropospheric water vapour and ENSO are evident.

1 Introduction

As the most important greenhouse gas in the troposphere water vapour plays a key role in the climate feedback loop. This feedback is known to amplify the already known greenhouse effect through an increase in CO_2 by about 60 % (Forster et al., 2007). Relevant for the climate is not only the water vapour distribution in the troposphere, but also the amount of water vapour in the stratosphere (Solomon et al., 2010). The abundance of stratospheric water vapour (SWV) is mainly controlled by the temperatures at the tropical tropopause (Mote et al., 1996). This leads to a high inter-annual and multi-decadal variability, mostly dominated by the Quasi-Biennial Oscillation (QBO) and El Niño-Southern Oscillation (ENSO), which both affect tropical tropopause temperatures. Besides the two well known phenomena also changes in the chemical balance (like

ACPD
15, 34407–34437, 2015

higher methane oxidation rates through an increase of stratospheric chlorine, hydroxyl and ozone), changes in circulation patterns, as well as volcanic influences have to be taken into account (Forster et al., 2007; Stenke and Grewe, 2005).

The effect of volcanoes on the climate system was investigated with models under different aspects. Stenchikov et al. (1998) addressed the radiative impact of Mount Pinatubo aerosols. They used observational data of aerosol extinctions and effective radii to calculate the radiative forcing with the ECHAM4 general circulation model and found that the stratospheric heating was mainly due to near-infrared solar forcing. Thomas et al. (2009a, b) were the first to use a comprehensive and complex simulation of the ECHAM5 general circulation model to evaluate the effects of the Mount Pinatubo eruption under different boundary conditions taking into account observed SSTs and volcanically induced ozone anomalies, as well as QBO and ENSO. They were able to realistically reproduce the observed lower stratospheric temperature response with the combined effects of the prescribed SSTs, ozone anomalies and the state of the QBO. Graf et al. (1993) used the ECHAM2 general circulation model to investigate the stratospheric aerosol effects of El Chichón and Mount Pinatubo on the Northern Hemisphere's (NH) climate. They identified short-term dynamical responses and a warming of the lower troposphere in the first winter season after the eruptions, which they found to be in good agreement with observations. With the MAECHAM4/CHEM model Timmreck and Graf (2006) performed a model study to simulate the radiative effects and the dispersal of the aerosols after the eruption of a super volcano in the mid-latitudes of the NH. They discovered that the initial dispersal of the aerosol cloud mainly depends on the season of the eruption. In summer, the cloud is transported west- and northward, in winter more south- and eastward. Contrary to the heating found in other studies after the Pinatubo eruption, Timmreck and Graf (2006) determined a strong cooling of $\sim -1.6\,\mathrm{K\,d^{-1}}$ in the upper stratosphere shortly after the eruption of the super volcano. The dispersal of the Mount Pinatubo aerosol cloud was investigated with the ECHAM4 model by Timmreck et al. (1999a) using a Newtonian relaxation technique. Their simulated aerosol distribution was mostly in good agreement with observational

ACPD
15, 34407–34437, 2015

data. Timmreck et al. (1999b) also used the ECHAM4 model to perform an interactive simulation with prognostic aerosols for the Mount Pinatubo eruption. They then compared the results for the years 1991 and 1992 with a non-interactive study, satellite observations and in situ measurements. They were able to reproduce dynamical effects in accordance with observations and found maximum heating rates of $\sim 0.3\,\mathrm{K\,d^{-1}}$ in October 1991.

Regarding the changes in stratospheric water vapour in the aftermath of major volcanic eruptions, Oltmans et al. (2000) found in the limited observational data available that there is a SWV increase after volcanic eruptions, which disappeared after approximately 2 years. Joshi and Jones (2009) proposed that within the following 2 years after the eruption, a heating of the tropopause layer imposed by volcanic aerosol clouds allowed more water vapour to pass into the stratosphere. They supposed that the total SWV perturbation (globally averaged) after the Mount Pinatubo eruption would account for at least 15 % more SWV. The increase in tropopause temperatures supported the investigations of Considine et al. (2001). They also made volcanic eruptions partly responsible for the SWV-trend in the 1990s. In their model simulation they determined an increase in tropopause temperatures of about 0.5 K, an increase in stratospheric temperatures of around 2–3 K at a height between 20 and 50 hPa and a maximum increase in water vapour of only ~ 6 % in the upper stratosphere after Mount Pinatubo.

The present study investigates the SWV perturbations of the major volcanic eruptions of El Chichón (Mexico, 1982) and Mount Pinatubo (Philippines, 1991) using the state of the art general circulation chemistry-climate model EMAC. The main objective is to analyse the perturbation of SWV and the transport paths of water vapour into the stratosphere. In Sect. 2 a brief description of the EMAC model and the setup of the used simulations are given. In Sect. 3 our results of volcanic SWV perturbations are presented. Section 4 discusses the results and Sect. 5 summaries the findings and provides an outlook on further studies.

ACPD
15, 34407–34437, 2015

2 Model simulations

2.1 Model description

The ECHAM/MESSy Atmospheric Chemistry (EMAC) model is a numerical chemistry and climate simulation system that includes sub-models describing tropospheric and middle atmosphere processes and their interaction with oceans, land and human influences (Jöckel et al., 2010). It uses the second version of the Modular Earth Submodel System (MESSy2) to link multi-institutional computer codes. The core atmospheric model is the 5th generation European Centre Hamburg general circulation model (Roeckner et al., 2006). For the present study we applied EMAC (ECHAM5 version 5.3.02, MESSy version 2.51) in the T42L90MA-resolution, i.e., with a spherical truncation of T42 (corresponding to a quadratic Gaussian grid of approx. 2.8° by 2.8° in latitude and longitude) with 90 vertical hybrid pressure levels up to 0.01 hPa.

2.2 ESCiMo consortial simulations

Multiple simulations with different boundary conditions were performed within the "Earth System Chemistry integrated Modelling (ESCiMo)" initiative (Jöckel et al., 2015). These model simulations were defined to improve the understanding of processes in the atmosphere and also to help answer questions related to climate change, ozone depletion and air quality. Besides the scientific relevance, the obtained results are supposed to have also political and social impact. This is especially important for the contribution to the WMO/UNEP ozone and IPCC climate assessments.

In our study we focus on 2 simulations with specified dynamics. They were "nudged" with a Newtonian relaxation technique towards 6 hourly ECMWF reanalysis data (ERA-Interim, Dee et al., 2011), which are available from the year 1979 to 2012.

The Newtonian relaxation (nudging) of the prognostic variables, divergence, vorticity, temperature and the (logarithm of the) surface pressure is applied in spectral space with a corresponding relaxation time of 48, 6, 24 and 24 h, respectively. The sea sur-

ACPD
15, 34407–34437, 2015

face temperatures (SSTs) and the sea ice concentrations (SICs) are prescribed every 12 h. A nudging of the "wave zero" (i.e., the global mean) temperature ($\overline{T}$) is, however, excluded. This allows a temperature response of the model. The nudging is applied in the troposphere from above the boundary layer up to 10 hPa. The nudging coefficients increase from zero in a vertical transition region with a maximum between 84 and 10 hPa and decrease again. The boundary layer (the lowest three model levels) and the middle atmosphere (less than 10 hPa) are left unaffected.

The simulations RC1SD-base-01 (in the following referred as VOL) and RC1SD-base-10 (from now on referred as NOVOL) range from 1979 to 2012 and 2013, respectively. They are nearly identical simulations, which differ mainly with respect to volcanic perturbations in the system: In VOL the volcanic perturbation is considered, whereas NOVOL has no volcanic perturbation, with the exception that the aerosol surfaces (which are relevant for the heterogeneous chemistry) are also prescribed in the NOVOL simulation. In VOL the dynamically relevant volcanic sulfate aerosol effect is achieved by prescribing zonally and monthly averaged values of the aerosol radiative properties: extinction coefficients for the 16 spectral bands (short wave: 4 bands, long wave: 12 bands) of EMAC, single scattering albedo and asymmetry factor (B. Luo, personal communication, 2013; ftp://iacftp.ethz.ch/pub_read/luo/ccmi/). These are used by the radiation scheme to calculate the corresponding heating rates (Fig. 1). Atmospheric chemistry in troposphere and stratosphere is calculated interactively. Volcanic temperature changes might therefore influence methane oxidation, a water vapour source, in the stratosphere.

The nudging data in some parts already include the dynamical effects of the volcanoes and therefore both simulations are influenced. The results in this study will mainly represent the difference between the VOL and NOVOL simulation, if not stated otherwise. This configuration allows a one-by-one comparison but still limits the analysis of the dynamical effects. Note, however, the hydrological cycle itself is "free running" and not nudged in the simulations.

ACPD
15, 34407–34437, 2015

The heating rates lead to increased local temperatures (Fig. 1), which cause perturbations in the atmospheric chemistry and dynamics (i.e., upward motion in the stratosphere). The dynamical effect in turn has an impact on the vertical distribution of chemical constituents and water vapour.

3 Perturbation of stratospheric water vapour

In this section we present the findings of our study of the perturbations of stratospheric water vapour for the time periods following the eruptions of El Chichón in 1982 and Mount Pinatubo in 1991. We first concentrate on tropical stratospheric aspects and then also take possible influences from the South Asian monsoon region into account as well as impacts on tropospheric water vapour and ENSO.

3.1 Tropics

The maximum heating rates for the tropical mean (5° S–5° N) for both volcanoes are found at a height of about 20 hPa with an amplitude of around 0.45 and 0.6 K d^{-1}, respectively (Fig. 1). For Mount Pinatubo there is a second local maximum of heating rates located around 40 hPa occurring approximately 3 months after the eruption. These maxima coincide well with the maxima of the aerosol extinction.

The overall larger values for the Mount Pinatubo eruption are explainable through the higher mass of ejected SO_2 (with a factor of 2–3) and therefore larger aerosol extinction, which lead to increased heating rates and stronger temperature changes (Figs. 1 and 2). The volcanically induced temperature increase has its maximum values in the middle stratosphere and reaches within the same month ∼ 1 K for El Chichón and ∼ 3 K for Mount Pinatubo, respectively, at 20 and 30 hPa. For the 50 hPa level the amplitude of the temperature change reaches about 1.5 K for El Chichón and 4 K for Mount Pinatubo, respectively, approximately 6 months after the eruptions. For both volcanoes the induced temperature increases decline back to unperturbed values within

ACPD
15, 34407–34437, 2015

about 2 years. Both volcanoes' signals are clearly evident in a difference plot. The signal of El Chichón is about half the standard deviation of the annual temperature variation, while that of Mount Pinatubo is larger than this amplitude (Fig. 2).

As the volcanic aerosols were mostly injected near the equator and their effects of increasing heating rates and temperatures are also concentrated in the tropical region, we find the main SWV perturbations in the tropical stratosphere as seen in Fig. 3 as a difference plot (VOL-NOVOL) for both volcanoes. The increased amount of water vapour in the stratosphere ranges from below the cold point at 90 up to 10 hPa and is located in the upwelling region of the Brewer–Dobson circulation (BDC) in the tropics.

Both volcanic periods show an increase in SWV shortly after the eruption compared to the simulation without volcanoes (NOVOL). The absolute maximum for El Chichón of around 0.3 ppmv[1] is located around 90 hPa and is reached approximately one year after the eruption in the NH summer season, whereas the increases in water vapour for Mount Pinatubo result in a double peak maximum. The first peak is located at a height of around 80 hPa some 9 months after the eruption and the second is propagating from near 100 hPa with a total increase of 1 ppmv starting one year after the eruption. The signals are then propagating similar to the tropical tape recorder to higher altitudes of the stratosphere.

The relative increases compared to the background values of NOVOL are up to 20 % for El Chichón at a height between 90 and 80 hPa occurring in the first winter after the eruption (Fig. 3). For Mount Pinatubo there is some kind of a triple peak structure of relative maxima around the same height, with the first maximum showing an increase of 40 % also in the first winter after the eruption. The second is following in the same year's summer season with a magnitude of 50 % increase in SWV and is tailed by a third local maximum in the following winter season (1992/93) with a relative increase of about 45 %.

The small local SWV maximum found between 20 and 30 hPa shortly after the eruption of El Chichón coincides with the local maximum of temperature increase of around

[1] 1 ppmv = 1 µmol mol^{-1} in SI units.

ACPD
15, 34407–34437, 2015

1 K (Fig. 1). Also the maximum of relative increases in water vapour around one year after the El Chichón eruption is related to the temperature increase of 1.5 K, which also occurs one year after the eruption at the same pressure level. Correspondingly, for Mount Pinatubo the absolute maximum of temperature increase can be found at a height of around 40 hPa in November 1991 to February 1992, where also a small absolute (around 0.3 ppmv) and a relative increase (around 10 %) in SWV occurs in the winter months after the eruption.

The negative values of water vapour changes found at a pressure level of around 50 hPa and above for both volcanoes are associated with the uplifting of air characterised by lower SWV mixing ratios through the additional volcanic heating in this area. The SWV minima are propagating similar to the tropical tape recorder to higher altitudes.

The time lag between the local maximum of induced heating and the propagation of the SWV signal into the same height is about 27–28 months for El Chichón and ~ 26 months for Mount Pinatubo.

As the tropopause is located within the area affected by the induced heating of the stratosphere, changes in cold point characteristics can be found in the simulation (Fig. 4). The cold point temperature increases with a maximum of around 1.4 and 2.4 K, respectively, approximately one year after the eruptions. The pressure at the cold point changes by up to 1 and 3 hPa, respectively, within 9–12 months. The specific humidity is also increasing with a maximum of about 0.25 and 0.55 $\times 10^{-6}$ kg kg^{-1}, respectively, approximately 18 months after both volcanic eruptions. With rising temperatures at the cold point more water vapour is transported into the stratosphere (Randel et al., 2004). The increased humidity at the cold point supports this conclusion. The displayed changes in pressure at the cold point can be explained through changes in the local temperature gradient, which differs between both simulations. Because of the temperature changes the local cold point is found around 1.2 and 3 hPa, respectively, below its unperturbed altitude.

ACPD
15, 34407–34437, 2015

Figure 5 shows the water vapour perturbation at the height of the local relative maxima at about 80 hPa. The time series shows a triple peak (compare relative changes of Fig. 3) of differences in absolute values for Mount Pinatubo. The first is occurring in late 1991, the second in the beginning of 1992 and the third in late 1992 with a maximum of about ~ 0.9 ppmv. For El Chichón the increase in water vapour at this height results in a longer lasting peak, starting shortly after the eruption and rising to a maximum of about 0.4 ppmv in late 1983. There is a small second maximum in mid 1984 with an amplitude of 0.2 ppmv.

Figure 6 represents a latitude-time cross-section for the changes in water vapour for both volcanic periods near the 90 hPa level. As it can be seen, the largest absolute increases of water vapour are in the extra-tropical region of the Northern Hemisphere. The maxima reach 0.6 ppmv for El Chichón and 1.2 ppmv for Mount Pinatubo, respectively, in the second year after the eruption. Both extra-tropical maxima are located mainly between 10 and 40° N. However, the maximum relative increase in SWV is in the tropics about 20 % for El Chichón and 40–50 % (a double peak) for Pinatubo compared to the background value of NOVOL. Interesting is also the periodicity of the maxima, especially for the El Chichón eruption, as it occurs in the NH summer months for the three summer seasons after the eruption. The Pinatubo period is similar to El Chichón, but lacks a third maximum in 1993.

These results underline the special importance of the extra-tropical region for the transport of water vapour into the stratosphere. This aspect will be addressed in the following section.

3.2 Monsoon and extra-tropical influences

Dessler et al. (1995) found in observational data that moist air is able to enter the stratosphere in subtropical regions by traveling along isentropic surfaces. Figure 7 shows latitude-height cross-sections for the NH summer months (June, July, August) one year after the eruption of El Chichón and Mount Pinatubo, respectively. The increase in SWV appears globally. Both volcanoes exhibit a strong signal around 20 to 40° N in the NH,

ACPD
15, 34407–34437, 2015

propagating through the tropopause into the stratosphere, and reaching a height of 90–80 hPa. The time period shown represents the SWV increases with mixing ratios of around 0.6 ppmv for El Chichón and 1.2 ppmv for Mount Pinatubo, respectively. As the temperature of the tropopause in the subtropics is far higher (around ~ 200–225 K) than in the tropics (normally below 190 K), the ascending air parcels are characterised by a higher saturation vapour pressure and therefore by a higher mixing ratio of water vapour leading to a moistening of the extra-tropical stratosphere.

Upward transport of water vapour occurs predominantly during the South Asian summer monsoon (SASM), which is determined as a significant source of moisture for the upper-level of the monsoon anticyclone and the lower extra-tropical stratosphere (Dethof et al., 1999; Eichinger et al., 2015). The SASM is located mainly over northern India, the Tibetan plateau, central Asia and China and is associated with strong seasonal circulation anomalies and the isolation of air masses, which starts in June and ends in September.

In the month of August, directly after both eruptions took place, a significant increase in SWV with a magnitude of one standard deviation (of the NOVOL simulation) showed up in that region until August of the second year (Fig. 8). The third year's August does not show any signs of a further increase. According to one of the "stratospheric fountains" (Newell and Gould-Stewart, 1981) the Asian summer monsoon can be accounted for increasing SWV amounts after volcanic eruptions through transport of water vapour from the troposphere into the stratosphere.

The large-scale circulation patterns of the SASM can reach deep into the subtropics and are primarily driven by thermal processes and linked to convective latent heating. These processes lead to an appearance of anticyclones in the upper troposphere and lower stratosphere, able to reach up to around 70 hPa (Dunkerton, 1995), and to an exchange of air masses through deep convection. The moist air passes the dynamical tropopause traveling along isentropes, which cross the tropopause in this region. Through the extent of the anticyclone into the lower stratosphere the air is not freeze-dried by passing regions with low temperatures. This moistening can only be found

ACPD
15, 34407–34437, 2015

in the NH and reaches its maximum in the boreal summer months, however, the total strength varies from year to year.

3.3 Influence on tropospheric water vapour and ENSO

In the first winter season after both eruptions increased amounts of water vapour propagate from the surface up to the tropopause. Because of the large background values compared to the stratosphere, the relative increase is small. The water vapour "column" reaches a pressure level of ~ 150 hPa. Large amounts of water vapour are able to penetrate the tropopause at the time with the largest increases in cold point temperature around one year after the eruptions (Fig. 4).

The water vapour anomalies in the troposphere coincide with ENSO-events, at least the signals beginning in the first December after the eruptions. El Niños are generally strongest in the season from December to April and have a large impact on the weather system. They result in increased tropical convection and general changes in the circulation around the tropical tropopause (upwelling) due to positive temperature effects. The occurring temperature perturbations can expand well above the tropopause into the stratosphere (see Scherllin-Pirscher et al., 2012 and references therein).

The increased temperatures also lead to more water vapour in the troposphere, which subsequently propagates into the stratosphere. Fueglistaler and Haynes (2005), as well as Scaife et al. (2003) therefore related El Niño situations with a moistening of the stratosphere. The volcanic eruptions occurred in spring before the El Niños developed in the turn of the years 1982–1983 and 1991–1992. Also the periods with increased negative values of the Southern-Oscillation-Index (SOI, indicating the tendency for El Niño events) after 1992 seem to coincide well with the increases in water vapour (Fig. 9).

After the volcanic eruptions the total available potential energy (CAPE) featured a drop (not shown). This results in a reduced convective activity due to an increase in atmospheric stability caused by the volcanic heating and the steeper temperature gradient in the upper troposphere. Less convection leads to a subsequent decrease

ACPD
15, 34407–34437, 2015

in precipitation and a weakening of the hydrological cycle. The water vapour in the atmosphere is not converted into precipitation and hence is transported to higher altitudes, where increased tropopause temperatures allow more water vapour to enter the stratosphere. This supposes that major volcanic eruptions influence El Niños and significantly amplify the moistening of the tropical stratosphere.

So far the results can be summarised that volcanic eruptions increase the concentrations of tropospheric and stratospheric water vapour. Increased temperatures and therefore higher saturation vapour pressures at the tropopause allow additional water vapour to transit into the stratosphere. There, the SWV gets dispersed along characteristic circulation patterns (i.e., BDC, tropical tape recorder and tropical pipe; Plumb, 1996). The values of water vapour in the stratosphere reach their peak after about 18 months and it takes the signal 3 to 4 years to decay.

4 Discussion

The volcanic forcing heats the lower stratosphere mainly in the tropical region, leading to an increase in temperatures for about 2 years after the eruptions with a maximum of 1.5 K for El Chichón and 4 K for Mount Pinatubo, respectively. Both can be identified as significant changes, though the overall temperature increase may be overestimated by our model by about 1 K.

Considine et al. (2001) used an interactive 2-D model simulation to evaluate the effects of the volcanic aerosols of Mount Pinatubo. They used observations of extinction rates, size distribution and aerosol surface area densities to simulate the aerosol effects. They also compared their resulting temperature changes after the eruption with the findings of Angell (1997), who used radiosonde data and removed QBO effects, and values from NCEP analysis on three different pressure levels (20, 30 and 50 hPa, see Fig. 8 of Considine et al., 2001). The results from Angell (1997) peaked with a temperature increase of approximately 3–4 K at a height between 30 and 50 hPa in late 1991, which agrees well with the results in the present study (Fig. 2 and also Fig. 1 in

ACPD
15, 34407–34437, 2015

Sect. 2.2) with a peak of 4 K occurring around 40 hPa between 1991 and 1992. Also the duration of the temperature signal of approximately 2 years is in agreement with the results presented here. This is supported by the simulation of Joshi and Shine (2003), who obtained similar results like in the NCEP analysis with a more complex GCM than the 2-D model of Considine et al. (2001). On 20 hPa it agrees better with the model of Considine et al. (2001), on 50 hPa however, better with the results from Angell (1997). The results exceed the regional standard deviation.

The stratospheric temperature increase leads to elevated temperatures at the cold point by about 1.4 and 2.4 K. The resulting higher saturation vapour pressure of the air allowed more water vapour to enter the stratosphere through the tropopause, leading to SWV increases in the tropics of 20 % for El Chichón and 50 % for Mount Pinatubo, respectively, in the lower stratosphere. Two (Mount Pinatubo) to 3 (El Chichón) summer seasons after the eruptions, the South Asian summer monsoon could be determined as a significant source of additional stratospheric moisture. In the NH summer months increased amounts of water vapour entered the stratosphere over the SASM anticyclone, peaking in the second year after the eruptions with an increase of 0.5 ppmv for El Chichón and 1 ppmv for Mount Pinatubo, respectively.

Considine et al. (2001) also studied the changes in stratospheric water vapour that occurred after the volcanic aerosol forcing of Mount Pinatubo. They mostly concentrated on changes in trends, but also showed the response of SWV perturbations in their model (their Fig. 16b) in a very similar way like in Fig. 3 in the previous section of our study.

Some of the facts of their figure are worth being pointed out: their model also simulated some kind of a double peak signal. The first peak occurring in early 1992 with its maximum (approximately a 30–35 % increase) at a height of ~ 80 hPa and a second peak in the change of year 1992–1993, with a signal that is smaller in magnitude (around 25 %). A comparable peak structure for the specific humidity changes was shown by Joshi and Shine (2003) for the NCEP analysis data (their Fig. 3, bottom), but their model wasn't able to reproduce this. They referred to Angell (1997) for an

ACPD
15, 34407–34437, 2015

explanation of the occurring double peak as an influence of the QBO. Both signals in Considine et al. (2001) are propagating into higher regions of the stratosphere, which is in good agreement with our model. Additionally, they also simulated a SWV minimum shortly after the eruption, which propagates from around 20 hPa higher into the stratosphere. The, to some extent, lower relative values can probably be explained through smaller temperature changes associated with the volcanic forcing. They also mentioned that HALOE H_2O data is lacking a clear signal of water vapour increase for the Mount Pinatubo period and therefore assumed that it may be possible that the simulated temperature changes at the tropopause, which control the entry value of water vapour in that region, are too high. They further concluded that in reality a Mount Pinatubo signal in tropopause temperatures was masked by the inter-annual variability of the tropopause of 1–2 K.

Joshi and Shine (2003) also found the maximum increases in their model over the equatorial regions, but their results did not indicate any sign of increased transport from the extra-tropical troposphere into the stratosphere (their Fig. 4). In our simulations the occurrence of a tropospheric drying[2] effect after volcanic eruptions is masked by the slight differences between the two used simulations (Fig. 9).

A comparison of our results with observations is difficult, because water vapour measurements prior to 1994 may be noisy and biased due to the volcanic aerosol layer (Fueglistaler, 2012). Interestingly, our results of the VOL simulation show a period with less water vapour compared to the NOVOL simulation without volcanic eruption (Fig. 3) directly after the eruption of Mount Pinatubo similar as present in the HALOE data shown by Fueglistaler (2012), his Fig. 5a. This period of reduced water vapour amount is also visible shortly after the eruption of El Chichón. We suggest that this effect is associated with the uplifting of air through the additional volcanic heating in this area.

Moreover, a significant increase of water vapour is propagating from the troposphere into the stratosphere during the El Niños in 1982–1983 and 1991–1992, in addition

[2]The drying results from decreasing tropospheric temperatures due to less absorption of solar radiation, which is "blocked" by the volcanic aerosols (e.g., Soden et al., 2002).

ACPD
15, 34407–34437, 2015

to the anyway elevated values during El Niños. The volcanic heating increased the upper tropospheric stability and therefore reduced the convective activity, which led to less precipitation and more available water vapour in the atmosphere. Once the water vapour signal reaches the stratosphere, it gets dissipated by the typical stratospheric circulation patterns of the BDC, the tropical pipe and the tropical tape recorder. An overview of the mainly affected tropospheric processes is given in Fig. 10.

The reaction of the model to the volcanic perturbation also resulted in dynamical changes on a sub-synoptic scale, which influenced the vertical and horizontal winds. Most changes were located within regions of altered water vapour abundance. Strengthening of vertical motion was found mainly in the tropical region in the stratosphere, resulting directly from local heating rates. The differences in vertical velocity accounted for about 0.1–0.2 10^{-3} Pa s^{-1} after the eruption of Mount Pinatubo. Though, these results have to be considered with care, as the simulations were influenced through the applied Newtonian relaxation technique, which affected the dynamical variables vorticity and divergence.

5 Summary and outlook

The two nudged simulations RC1SD-base-01 (with volcanic perturbation, VOL) and RC1SD-base-10 (no volcanic perturbation, NOVOL) were used to carry out a sensitivity analysis of the effects of two major volcanic eruptions (El Chichón and Mount Pinatubo) on stratospheric water vapour (SWV). To simulate the effects of the volcanic eruptions, the VOL simulation used prescribed monthly and zonally averaged optical properties (optical thickness, asymmetry factor and single scattering albedo) of the volcanic aerosol. These were derived from observational data and used in the model to calculate the heating rates, which result in thermal, dynamical and chemical changes. The nudging setup was chosen to allow a temperature response to the volcanic aerosol driven heating. Here the effects on the hydrological cycle, in particular the SWV distribution and time development, was investigated.

ACPD
15, 34407–34437, 2015

Our results are in good agreement with findings from other literature, especially in structure and duration of the volcanic signals. We found increased amounts of water vapour in the stratosphere shortly after the eruptions, which propagate into higher regions of the stratosphere. The South-Asian summer monsoon (SASM) was identified as a source of additional SWV for at least two years after the eruptions. Additionally, the burden of tropospheric water vapour was increased during the El Niños of 1982/83 and 1991/92. Because of a weakened hydrological cycle (i.e., less precipitation) and increased temperatures at the tropopause the water vapour was able to propagate into the stratosphere. In conclusion, strong volcanic eruptions block the sun by the injection of aerosol particles into the stratosphere, where they remain for years leading to a cooling of the surface. Locally these aerosols heat the middle stratosphere down to the tropopause and subsequently increase the amount of water vapour transported into the stratosphere. Additionally, periods of strong convective activity (e.g., El Niños) in the tropics are influenced by the stabilisation of the vertical temperature gradient. Thus, the modification of the atmospheric water vapour comprises not only the stratosphere but the whole vertical column. Our focus in this study was the estimation of SWV increases and the related transport paths. Volcanic eruptions, however, also influence chemical processes in the stratosphere. For instance the ozone generation is influenced by temperature changes. Moreover, SWV formed by methane oxidation as a source of SWV needs further investigation.

Acknowledgements. This study was supported by the German Research Foundation (DFG) Research Unit FOR 1095 “Stratospheric Change and its Role for Climate Prediction” (SHARP) under the grant number JO 757/1-2. We acknowledge the use of the tool cdo (https://code.zmaw.de/projects/cdo) for the processing of data and the program Ferret from NOAA’s Pacific Marine Environmental Laboratory (http://ferret.pmel.noaa.gov) for analysis and creation of graphics in this study. We further thank the German Climate Computing Centre (DKRZ) for providing computational capacities for data processing and analysis.

The article processing charges for this open-access publication were covered by a Research Centre of the Helmholtz Association.

ACPD
15, 34407–34437, 2015

References

Angell, J. K.: Stratospheric warming due to Agung, El Chichón, and Pinatubo taking into account the quasi-biennial oscillation, J. Geophys. Res.-Atmos., 102, 9479–9485, doi:10.1029/96JD03588, 1997. 34419, 34420

Considine, D. B., Rosenfield, J. E., and Fleming, E. L.: An interactive model study of the influence of the Mount Pinatubo aerosol on stratospheric methane and water trends, J. Geophys. Res.-Atmos., 106, 27711–27727, doi:10.1029/2001JD000331, 2001. 34410, 34419, 34420, 34421

Dee, D. P., Uppala, S. M., Simmons, A. J., Berrisford, P., Poli, P., Kobayashi, S., Andrae, U., Balmaseda, M. A., Balsamo, G., Bauer, P., Bechtold, P., Beljaars, A. C. M., van de Berg, L., Bidlot, J., Bormann, N., Delsol, C., Dragani, R., Fuentes, M., Geer, A. J., Haimberger, L., Healy, S. B., Hersbach, H., Hólm, E. V., Isaksen, L., Kållberg, P., Köhler, M., Matricardi, M., McNally, A. P., Monge-Sanz, B. M., Morcrette, J.-J., Park, B.-K., Peubey, C., de Rosnay, P., Tavolato, C., Thépaut, J.-N., and Vitart, F.: The ERA-Interim reanalysis: configuration and performance of the data assimilation system, Q. J. Roy. Meteor. Soc., 137, 553–597, 2011. 34411

Dessler, A. E., Hintsa, E. J., Weinstock, E. M., Anderson, J. G., and Chan, K. R.: Mechanisms controlling water vapor in the lower stratosphere: "A tale of two stratospheres", J. Geophys. Res.-Atmos., 100, 23167–23172, doi:10.1029/95JD02455, 1995. 34416

Dethof, A., O'Neill, A., Slingo, J. M., and Smit, H. G. J.: A mechanism for moistening the lower stratosphere involving the Asian summer monsoon, Q. J. Roy. Meteor. Soc., 125, 1079–1106, doi:10.1002/qj.1999.49712555602, 1999. 34417

Dunkerton, T. J.: Evidence of meridional motion in the summer lower stratosphere adjacent to monsoon regions, J. Geophys. Res.-Atmos., 100, 16675–16688, doi:10.1029/95JD01263, 1995. 34417

Eichinger, R., Jöckel, P., and Lossow, S.: Simulation of the isotopic composition of stratospheric water vapour – Part 2: Investigation of HDO/H_2O variations, Atmos. Chem. Phys., 15, 7003–7015, doi:10.5194/acp-15-7003-2015, 2015. 34417

Forster, P., Ramaswamy, V., Artaxo, P., Berntsen, T., Betts, R., Fahey, D., Haywood, J., Lean, J., Lowe, D., Myhre, G., Nganga, J., Prinn, R., Raga, G., Schulz, M., and van Dorland, R.: Changes in atmospheric constituents and in radiative forcing, in: Climate Change 2007: The Physical Science Basis. Contribution of Working Group I to the Fourth Assessment Re-

ACPD
15, 34407–34437, 2015

port of the Intergovernmental Panel on Climate Change, edited by: Solomon, S., Qin, D., Manning, M., Chen, Z., Marquis, M., Averyt, K., Tignor, M., and Miller, H., Cambridge University Press, Cambridge, UK and New York, NY, USA, chap. 2, 129–234, available at: http://www.ipcc.ch/publications_and_data/publications_ipcc_fourth_assessment_report_wg1_report_the_physical_science_basis.htm (last access: 7 December 2015), 2007. 34408, 34409

Fueglistaler, S.: Stepwise changes in stratospheric water vapor, J. Geophys. Res.-Atmos., 117, 1–11, doi:10.1029/2012JD017582, 2012. 34421

Fueglistaler, S. and Haynes, P. H.: Control of interannual and longer-term variability of stratospheric water vapor, J. Geophys. Res.-Atmos., 110, D24108, doi:10.1029/2005JD006019, 2005. 34418

Graf, H., Kirchner, I., Robock, A., and Schult, I.: Pinatubo eruption winter climate effects: model versus observations, Clim. Dynam., 9, 81–93, 1993. 34409

Jöckel, P., Kerkweg, A., Pozzer, A., Sander, R., Tost, H., Riede, H., Baumgaertner, A., Gromov, S., and Kern, B.: Development cycle 2 of the Modular Earth Submodel System (MESSy2), Geosci. Model Dev., 3, 717–752, doi:10.5194/gmd-3-717-2010, 2010. 34411

Jöckel, P., Tost, H., Pozzer, A., Kunze, M., Kirner, O., Brenninkmeijer, C. A. M., Brinkop, S., Cai, D. S., Dyroff, C., Eckstein, J., Frank, F., Garny, H., Gottschaldt, K.-D., Graf, P., Grewe, V., Kerkweg, A., Kern, B., Matthes, S., Mertens, M., Meul, S., Neumaier, M., Nützel, M., Oberländer-Hayn, S., Ruhnke, R., Runde, T., Sander, R., Scharffe, D., and Zahn, A.: Earth System Chemistry Integrated Modelling (ESCiMo) with the Modular Earth Submodel System (MESSy, version 2.51), Geosci. Model Dev. Discuss., 8, 8635–8750, doi:10.5194/gmdd-8-8635-2015, 2015. 34411

Joshi, M. M. and Jones, G. S.: The climatic effects of the direct injection of water vapour into the stratosphere by large volcanic eruptions, Atmos. Chem. Phys., 9, 6109–6118, doi:10.5194/acp-9-6109-2009, 2009. 34410

Joshi, M. M. and Shine, K. P.: A GCM study of volcanic eruptions as a cause of increased stratospheric water vapor, J. Climate, 16, 3525–3534, 2003. 34420, 34421

Mote, P. W., Rosenlof, K. H., McIntyre, M. E., Carr, E. S., Gille, J. C., Holton, J. R., Kinnersley, J. S., Pumphrey, H. C., Russell, J. M., and Waters, J. W.: An atmospheric tape recorder: the imprint of tropical tropopause temperatures on stratospheric water vapor, J. Geophys. Res.-Atmos., 101, 3989–4006, doi:10.1029/95JD03422, 1996. 34408

ACPD
15, 34407–34437, 2015

Newell, R. E. and Gould-Stewart, S.: A stratospheric fountain?, J. Atmos. Sci., 38, 2789–2796, 1981. 34417

Oltmans, S. J., Vömel, H., Hofmann, D. J., Rosenlof, K. H., and Kley, D.: The increase in stratospheric water vapor from balloonborne, frostpoint hygrometer measurements at Washington, D. C., and Boulder, Colorado, Geophys. Res. Lett., 27, 3453–3456, doi:10.1029/2000GL012133, 2000. 34410

Plumb, R. A.: A "tropical pipe" model of stratospheric transport, J. Geophys. Res.-Atmos., 101, 3957–3972, doi:10.1029/95JD03002, 1996. 34419

Randel, W. J., Wu, F., Oltmans, S. L., Roselos, K., and Nedoluha, G. E.: Interannual changes of stratospheric water vapor and correlations with tropical tropopause temperatures, J. Atmos. Sci., 61, 2133–2148, doi:10.1029/95JD03422, 2004. 34415

Roeckner, E., Brokopf, M., Esch, M., Giorgetta, M., Hagemann, S., Kornblueh, L., Manzini, E., Schlese, U., and Schulzweida, U.: Sensitivity of simulated climate to horizontal and vertical resolution in the ECHAM5 atmosphere model, J. Climate, 19, 3771–3791, 2006. 34411

Scaife, A. A., Butchart, N., Jackson, D. R., and Swinbank, R.: Can changes in ENSO activity help to explain increasing stratospheric water vapor?, Geophys. Res. Lett., 30, 1880, doi:10.1029/2003GL017591, 2003. 34418

Scherllin-Pirscher, B., Deser, C., Ho, S.-P., Chou, C., Randel, W., and Kuo, Y.-H.: The vertical and spatial structure of ENSO in the upper troposphere and lower stratosphere from GPS radio occultation measurements, Geophys. Res. Lett., 39, L20801, doi:10.1029/2012GL053071, 2012. 34418

Soden, B. J., Wetherald, R. T., Stenchikov, G. L., and Robock, A.: Global cooling after the eruption of Mount Pinatubo: a test of climate feedback by water vapor, Science, 296, 727–730, 2002. 34421

Solomon, S., Rosenlof, K. H., Portmann, R. W., Daniel, J. S., Davis, S. M., Sanford, T. J., and Plattner, G.-K.: Contributions of stratospheric water vapor to decadal changes in the rate of global warming, Science, 327, 1219–1223, doi:10.1126/science.1182488, 2010. 34408

Stenchikov, G. L., Kirchner, I., Robock, A., Graf, H.-F., Antuña, J. C., Grainger, R. G., Lambert, A., and Thomason, L.: Radiative forcing from the 1991 Mount Pinatubo volcanic eruption, J. Geophys. Res.-Atmos., 103, 13837–13857, doi:10.1029/98JD00693, 1998. 34409

Stenke, A. and Grewe, V.: Simulation of stratospheric water vapor trends: impact on stratospheric ozone chemistry, Atmos. Chem. Phys., 5, 1257–1272, doi:10.5194/acp-5-1257-2005, 2005. 34409

ACPD
15, 34407–34437, 2015

Thomas, M. A., Timmreck, C., Giorgetta, M. A., Graf, H.-F., and Stenchikov, G.: Simulation of the climate impact of Mount Pinatubo eruption using ECHAM5 – Part 1: Sensitivity to the modes of atmospheric circulation and boundary conditions, Atmos. Chem. Phys., 9, 757–769, doi:10.5194/acp-9-757-2009, 2009a. 34409

Thomas, M. A., Giorgetta, M. A., Timmreck, C., Graf, H.-F., and Stenchikov, G.: Simulation of the climate impact of Mount Pinatubo eruption using ECHAM5 – Part 2: Sensitivity to the phase of the QBO and ENSO, Atmos. Chem. Phys., 9, 3001–3009, doi:10.5194/acp-9-3001-2009, 2009b. 34409

Timmreck, C. and Graf, H.-F.: The initial dispersal and radiative forcing of a Northern Hemisphere mid-latitude super volcano: a model study, Atmos. Chem. Phys., 6, 35–49, doi:10.5194/acp-6-35-2006, 2006. 34409

Timmreck, C., Graf, H.-F., and Feichter, J.: Simulation of Mount Pinatubo volcanic aerosol with the Hamburg climate model ECHAM4, Theor. Appl. Climatol., 62, 85–108, 1999a. 34409

Timmreck, C., Graf, H.-F., and Kirchner, I.: A one and half year interactive MA/ECHAM4 simulation of Mount Pinatubo Aerosol, J. Geophys. Res.-Atmos., 104, 9337–9359, 1999b. 34410

ACPD
15, 34407–34437, 2015

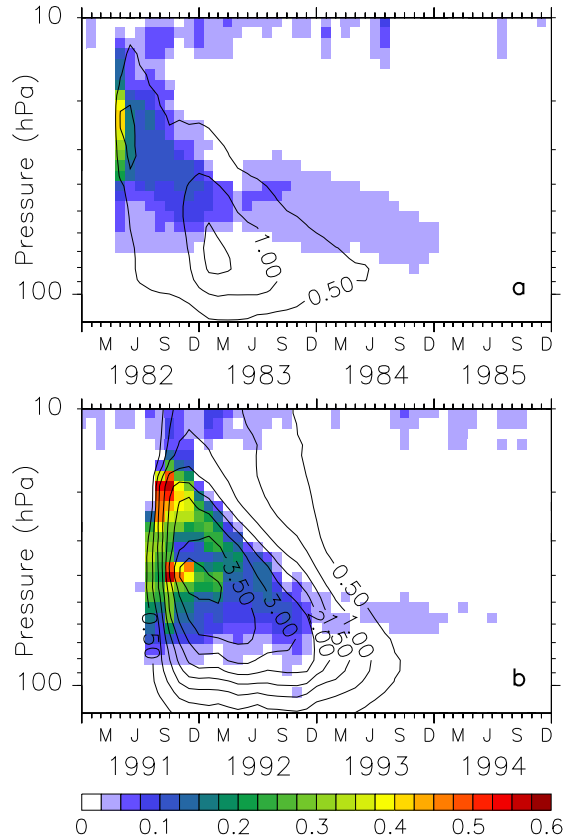

Figure 1. Zonally averaged heating rates [K d^{-1}] as differences (VOL-NOVOL) in the tropics (5° S–5° N) for **(a)** the 1982 El Chichón and **(b)** the 1991 Mount Pinatubo eruption. Contours indicate absolute temperature changes (interval 0.5 K) due to the heating rates.

ACPD
15, 34407–34437, 2015

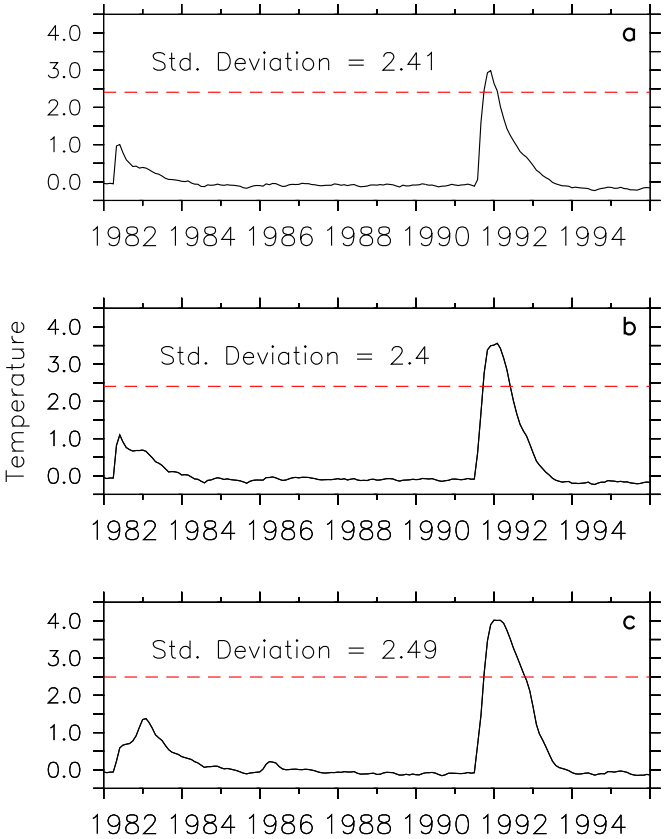

Figure 2. Temperature [K] differences (VOL-NOVOL) for the tropics (5° S–5° N), zonally averaged after the March 1982 El Chichón and the June 1991 Mount Pinatubo eruption for **(a)** 20 hPa, **(b)** 30 hPa and **(c)** 50 hPa. Red dashed lines indicate the standard deviation [K] for the unperturbed NOVOL simulation in the same region, calculated over the whole time series of 1979–2013.

ACPD
15, 34407–34437, 2015

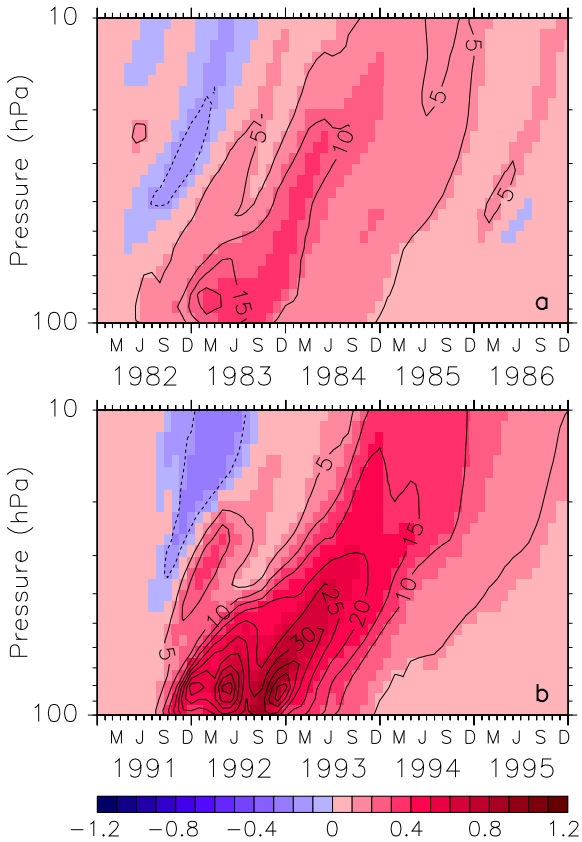

Figure 3. SWV [ppmv, colours] as absolute differences (VOL-NOVOL) in the tropics (5° S–5° N), zonally averaged for **(a)** the 1982 El Chichón and **(b)** the 1991 Mount Pinatubo eruption. Contours indicate relative changes of water vapour (interval 5 %) compared to the background value of NOVOL. The small signal seen in 1986 is associated with the November 1985 eruption of Nevado del Ruiz (Colombia).

ACPD
15, 34407–34437, 2015

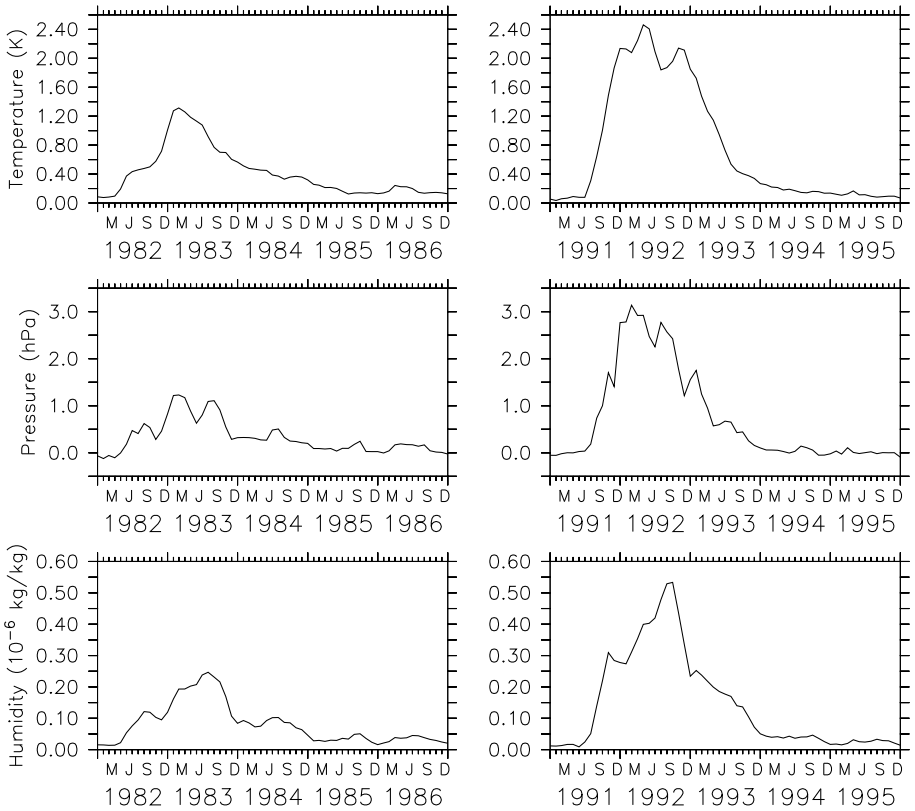

Figure 4. Zonally averaged differences (VOL-NOVOL) in temperature, pressure and humidity at the cold point in the tropics (5° S–5° N), zonally averaged for the El Chichón period (left) and the Mount Pinatubo period (right).

ACPD
15, 34407–34437, 2015

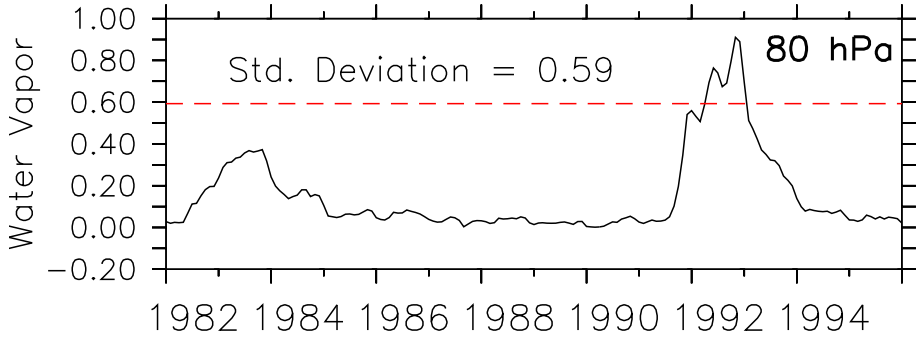

Figure 5. Differences (VOL-NOVOL) in water vapour [ppmv] for the tropics (5° S–5° N), zonally averaged after the March 1982 El Chichón and the June 1991 Mount Pinatubo eruption for the 80 hPa level. The red dashed line indicates the standard deviation [ppmv] for the unperturbed NOVOL simulation in the same region, calculated over the whole time series of 1979–2013.

ACPD
15, 34407–34437, 2015

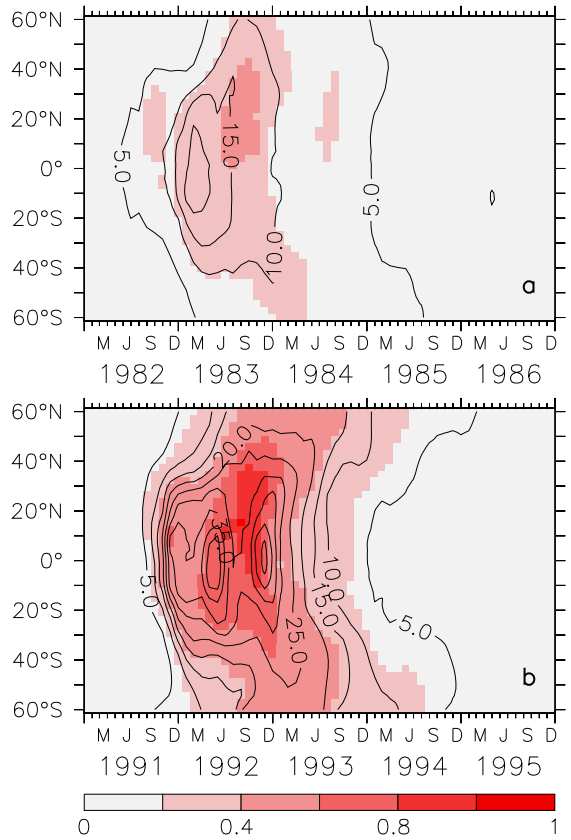

Figure 6. SWV [ppmv, colours] as absolute differences (VOL-NOVOL) zonally averaged near the 90 hPa level for **(a)** the El Chichón period (1982–1986) and **(b)** the Mount Pinatubo period (1991–1995). Contours indicate relative changes in water vapour (interval 5 %) compared to the background value of NOVOL. The small signal seen in 1986 is associated with the November 1985 eruption of Nevado del Ruiz (Colombia).

ACPD
15, 34407–34437, 2015

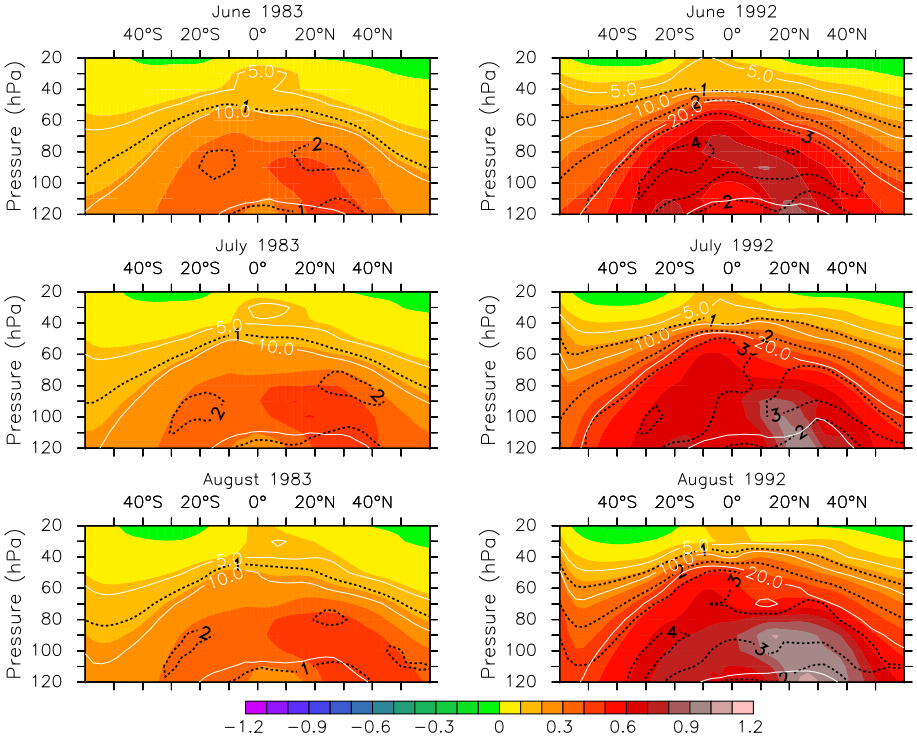

Figure 7. SWV [ppmv, colours] as absolute differences (VOL-NOVOL), zonally averaged as a near global (60° S–60° N) vertical cross-section at a height between 120 and 20 hPa for the months of June, July and August in the year following the eruptions (1983 and 1992, respectively). White contours indicate the relative increase in SWV (intervals 5, 10, 20 and 50 %) compared to the background value of NOVOL. Black dashed contours mark increases in units of standard deviation for the particular month in NOVOL (calculated over the time period 1979–2013). The left column shows the El Chichón period, the right column the Mount Pinatubo period.

ACPD
15, 34407–34437, 2015

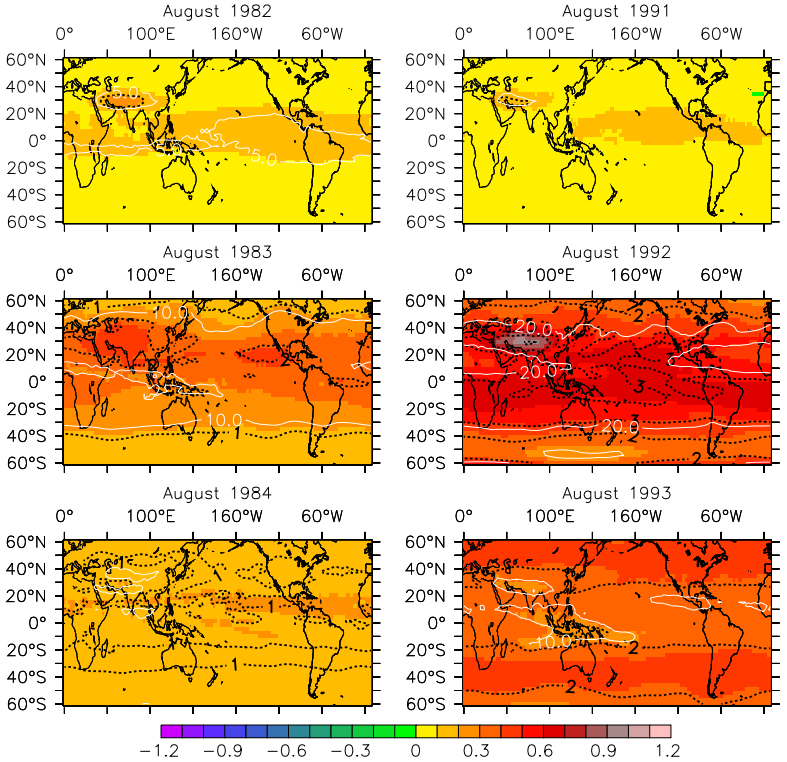

Figure 8. SWV [ppmv, colours] as absolute differences (VOL-NOVOL) as a near global (60° S–60° N) horizontal cross-section at 75 hPa for the month of August in the year of the eruptions and in the following two years. White contours indicate the relative increase in SWV (intervals 5, 10, 20 and 50 %) compared to the background value of NOVOL. Black dashed contours mark significant increases in units of standard deviation for the month of August in NOVOL (calculated over the time period 1979–2013). The left column shows the El Chichón period, the right column the Mount Pinatubo period.

ACPD
15, 34407–34437, 2015

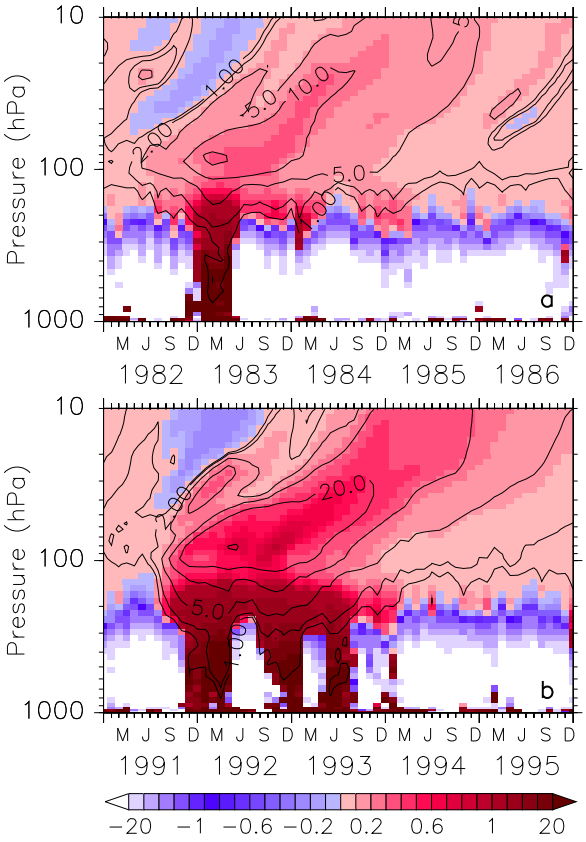

Figure 9. Same as Fig. 3 but for 1000–10 hPa with nearly logarithmic contour intervals from 1 to 20 %.

ACPD
15, 34407–34437, 2015

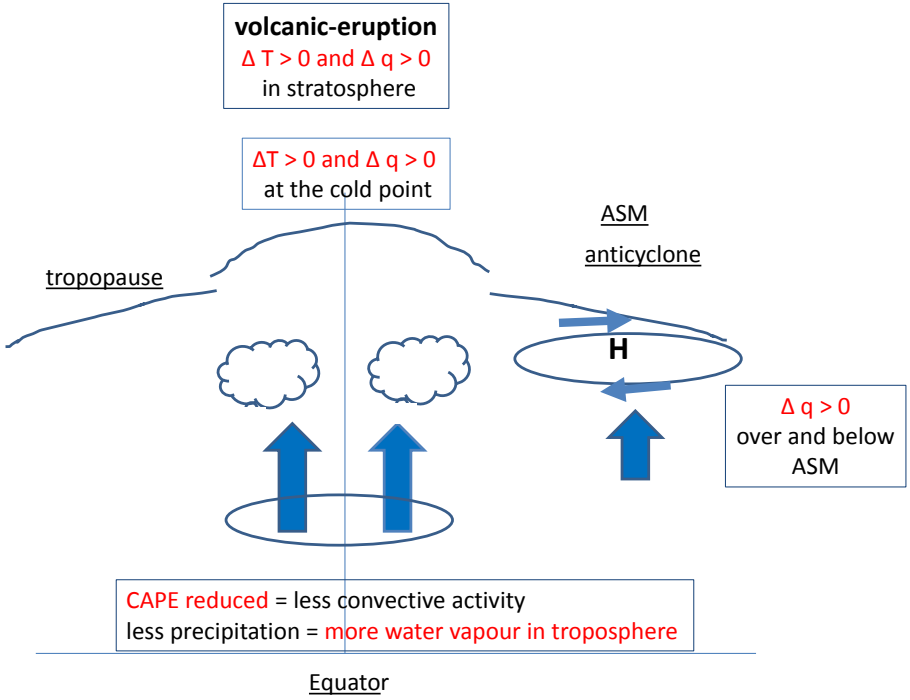

Figure 10. Schematic of tropospheric processes influenced by a strong volcanic eruption.

ACPD
15, 34407–34437, 2015